Research Square

Preprints are preliminary reports that have not undergone peer review.
They should not be considered conclusive, used to inform clinical practice,
or referenced by the media as validated information.

Potato common scab suppression by Bacillus velezensis 199 and asparagine is associated with tuber skin microbiome changes

yuxiao zeng
Yunnan Agricultural University
Subinur Emer
Agricultural Genomics Institute at Shenzhen
Bo Zhang
Agricultural Genomics Institute at Shenzhen
Tao Yang
Agricultural Genomics Institute at Shenzhen
Qian Tao
Agricultural Genomics Institute at Shenzhen
Shuai Luo
Agricultural Genomics Institute at Shenzhen
Jialin Rao
Agricultural Genomics Institute at Shenzhen
Xingyao Xiong
Agricultural Genomics Institute at Shenzhen
Yunyue Wang
Yunnan Agricultural University
Xu Cheng
chengxu@caas.cn

Agricultural Genomics Institute at Shenzhen

Research Article

Keywords: Bacillus velezensis, potato common scab, asparagine, tuber skin microbiome, synthetic community

Posted Date: November 20th, 2026

DOI: https://doi.org/10.21203/rs.3.rs-11537688/v1

License: This work is licensed under a Creative Commons Attribution 4.0 International License.
Read Full License

Additional Declarations: No competing interests reported.

Abstract

Potato common scab (PCS), caused by pathogenic *Streptomyces* spp., severely reduces potato tuber quality and commercial value. Although *Bacillus velezensis* has been widely investigated as a biocontrol agent against PCS, the responses of the tuber skin microbiome to *Bacillus*-based treatments, particularly the enrichment of bacteria with antagonistic potential, remain poorly understood. In this study, we identified *B. velezensis* 199 as a promising biocontrol strain against PCS and investigated its disease-suppressive activity and associated changes in the tuber skin microbiome. Strain 199 and its cell-free supernatant inhibited *Streptomyces acidiscabies* growth in vitro and reduced common scab severity under greenhouse conditions. Metabolomic profiling identified asparagine (Asn) as a candidate extracellular metabolite, with targeted quantification revealing an Asn concentration of approximately 9.4 µg/mL in the cell-free supernatant of strain 199. Exogenous Asn also inhibited *S. acidiscabies* growth in vitro and reduced disease severity under greenhouse conditions. Tuber skin microbiome analysis revealed shifts in bacterial community composition following treatment with strain 199, its cell-free supernatant, or Asn, with 13 bacterial amplicon sequence variants (ASVs) significantly enriched across all three treatments. Notably, a *Pandoraea* sp. isolate corresponding to one of the 13 shared enriched ASVs (ASV1676) exhibited antagonistic activity against *S. acidiscabies* in vitro. Together, these findings demonstrate that *B. velezensis* 199 and exogenous Asn suppress potato common scab and reshape the tuber skin microbiome, including the enrichment of an ASV associated with an antagonistic bacterial isolate. This study highlights the association between *Bacillus*-based biocontrol treatments and tuber skin bacterial communities, providing insights into the ecological responses accompanying PCS suppression.

Background

Potato (*Solanum tuberosum* L.) is the third most important food crop worldwide and provides carbohydrates, vitamins, minerals, and dietary fiber for human consumption (Devaux et al. 2014). As the harvested tuber represents the primary economic product of potato cultivation, diseases affecting tuber quality can substantially reduce market value and profitability. Potato common scab (PCS) is one of the most widespread tuber diseases and has attracted increasing attention because of its detrimental effects on tuber appearance and marketability. The disease primarily affects potato tubers, resulting in superficial, raised, and pitted lesions (Loria et al. 2006; Patel et al. 2026). Although PCS rarely causes plant death or substantial yield losses, the deterioration of tuber quality leads to significant economic losses in potato-producing regions worldwide (Zhao et al. 2022). For example, PCS has been reported to cause substantial economic losses in several potato-producing regions, where disease incidence remains widespread (Hill and Lazarovits 2005). These quality-related losses highlight the need for disease management strategies that protect tuber health and maintain the commercial value of potato production.

PCS is caused by pathogenic species of the soilborne, Gram-positive, filamentous bacterial genus *Streptomyces* (Dahal et al. 2019). The pathogenicity of PCS-causing *Streptomyces* spp. is mainly

associated with thaxtomins, a family of phytotoxins produced by pathogenic strains (Doumbou et al. 1998). Thaxtomin A, the major virulence determinant, disrupts cellulose biosynthesis and cell wall formation in developing tubers, resulting in abnormal cell expansion, suberization, and lesion formation (Biessy and Filion 2022). Although the molecular mechanisms of thaxtomin biosynthesis and pathogenicity have been extensively studied, disease development is also influenced by soil conditions, host genotype, and the surrounding microbial community (Shi et al. 2019). These features make PCS difficult to control under field conditions. Current management strategies include irrigation during tuber initiation, crop rotation, soil fumigation, soil acidification, foliar applications, and the use of resistant or tolerant potato cultivars (Dees and Wanner 2012; Cao et al. 2025). However, the effectiveness of these approaches is often inconsistent due to the long-term persistence of pathogenic *Streptomyces* in soil and the strong influence of environmental factors. Furthermore, chemical control measures are increasingly restricted because of environmental concerns and limited efficacy under field conditions (Majeed and Muhammad 2020). Therefore, sustainable and environmentally friendly strategies for PCS management are urgently needed. Plant growth-promoting rhizobacteria (PGPRs) can promote plant growth, alleviate abiotic stress, and protect plants against pathogen infection (Berendsen et al. 2012; Wang et al. 2021; He et al. 2024). Among PGPRs, members of the genus *Bacillus* have attracted considerable attention because of their strong environmental adaptability, endospore-forming capacity, and ability to produce a wide range of antimicrobial compounds (Jiang et al. 2025; Rabbee et al. 2019). Among *Bacillus*, *Bacillus velezensis* is recognized as an effective biocontrol species capable of suppressing multiple plant diseases through the production of lipopeptides, polyketides, hydrolytic enzymes, and volatile organic compounds, as well as through the induction of host resistance (Rabbee et al. 2023; Rabbee and Baek 2020; Zhong et al. 2024). Beyond direct antagonism, increasing evidence suggests that *Bacillus*-based biocontrol may also be associated with changes in plant-associated microbial communities. A recent study demonstrated that *Bacillus subtilis* XT11 suppressed potato common scab and altered the microbial community structure of potato geocaulosphere soil (Liu et al. 2026). However, given that potato common scab primarily affects developing tubers, the effects of *B. velezensis* on the tuber skin microbiome, particularly its association with the enrichment of bacteria exhibiting antagonistic activity against pathogenic *Streptomyces*, remain poorly understood.

In this study, we first screened and identified *Bacillus velezensis* 199 as a promising biocontrol strain against PCS. We subsequently demonstrated the antagonistic activity of its cell-free supernatant against *S. acidiscabies* and performed untargeted metabolomic profiling and targeted quantification to identify asparagine (Asn) as a candidate extracellular metabolite. We then evaluated the disease-suppressive effects of strain 199, its cell-free supernatant, and exogenous Asn under greenhouse conditions, with the field performance of strain 199 further assessed across different potato cultivars. To investigate the microbiome responses associated with these treatments, we characterized the bacterial communities of potato tuber skin and identified shared enriched amplicon sequence variants (ASVs) across the three treatments. Finally, we isolated a culturable bacterium corresponding to one of these ASVs and evaluated its antagonistic activity against *S. acidiscabies* in vitro. Together, this study provides insights

into the relationship between *B. velezensis*-based biocontrol treatments, extracellular Asn, and tuber skin microbiome changes associated with PCS suppression.

Results

Strain 199 exhibits the strongest antagonistic activity among screened Bacillus isolates

To identify *Bacillus* isolates with antagonistic activity against the potato common scab pathogen, 51 laboratory-preserved *Bacillus* isolates were screened using a plate antagonism assay with *S. acidiscabies*. The inhibitory effects varied markedly among the tested isolates. Several isolates formed visible inhibition zones around the colonies, indicating their ability to inhibit *S. acidiscabies* growth in vitro, whereas no inhibition zone was observed in the TSB control (Fig. 1A). The diameters of the inhibition zones were then measured and statistically analyzed. Among all tested isolates, strain 199 produced the largest inhibition zone, with a diameter of approximately 2.8 cm, which was markedly larger than those of the other isolates. In addition to strain 199, isolates P1F1, 105, 86, 29, S1, S7, S23, S27, and S28 also showed relatively strong antagonistic activity, with inhibition zone diameters greater than 1.0 cm (Fig. 1B). These results demonstrate that strain 199 possesses the strongest direct antagonistic activity against *S. acidiscabies* among the tested *Bacillus* isolates. Therefore, strain 199 was selected as a promising biocontrol candidate for subsequent evaluation of its disease-suppressive efficacy and antagonistic mechanisms.

Genomic features of strain B. velezensis 199

To clarify the taxonomic identity of strain 199 within the genus *Bacillus*, we performed genome-based phylogenetic analysis using representative genomes of closely related *Bacillus* species. The phylogenomic tree showed that strain 199 clustered within the *Bacillus velezensis* lineage and formed a well-supported clade with previously characterized strains, including AP46, FZB42, CBMB205, PEBA20, PD9, and HN10, while being clearly separated from other *Bacillus* species such as *B. subtilis*, *B. altitudinis*, and *B. cereus* (**Fig. S1**). Consistent with the phylogenomic placement, the average nucleotide identity (ANI) values between strain 199 and representative *B. velezensis* genomes ranged from 97.99% to 99.99%, supporting its assignment to *B. velezensis*.

To investigate the genomic basis underlying the antagonistic potential of strain 199, we analyzed its complete genome. The assembled genome consisted of a single circular chromosome of 3,888,177 bp, with a GC content of 46.4%. A total of 3,821 coding sequences (CDSs), 14 tRNA genes, and 3 rRNA genes were predicted. The circular genome map of strain 199 was generated using CGView (Fig. 2A). Functional annotation based on the COG database showed that a large proportion of CDSs were assigned to metabolism-related categories, whereas 24.4% of the CDSs were assigned to the category of unknown function. Among the annotated COG categories, “amino acid transport and metabolism” represented the most abundant category (n = 323), followed by “translation, ribosomal structure and biogenesis” (n = 304) and “carbohydrate transport and metabolism” (n = 249) (Fig. 2B). KEGG pathway annotation further revealed that genes involved in carbohydrate metabolism were the most abundant (n

= 266), followed by genes associated with amino acid metabolism (n = 222), vitamin metabolism (n = 175), and membrane transport (n = 160) (Fig. 2C). These results indicate that strain 199 possesses broad metabolic capacities, particularly in carbohydrate and amino acid metabolism, which may support its adaptation to plant-associated niches and its ability to produce or modulate bioactive metabolites.

Secondary metabolites produced by *Bacillus* spp. play important roles in suppressing phytopathogens and mediating plant-microbe interactions (Fazle Rabbee and Baek 2020). To evaluate the secondary metabolite biosynthetic potential of strain 199, we analyzed its genome using antiSMASH. A total of 17 putative secondary metabolite biosynthetic gene clusters were identified in the genome of strain 199 (Table 1). These clusters included NRPS, transAT-PKS, T2PKS, T3PKS, PKS-like, lanthipeptide-class-II, terpene, terpene-precursor, NRP-metallophore and RiPP-like clusters. Among these predicted clusters, nine were associated with secondary metabolites commonly found in *Bacillus* species and known to possess antimicrobial activity. These included gene clusters related to the biosynthesis of fengycin, bacillaene, macrolactin, bacilysin, bacillibactin, difficidin, plipastatin and surfactin. Taken together, the genome of strain 199 harbors multiple biosynthetic gene clusters associated with antimicrobial secondary metabolites, providing a genetic basis for its antagonistic activity against the potato common scab pathogen and its potential application as a biocontrol agent.

Table 1
antiSMASH analysis of strain 199

Cluster ID	Type of cluster	Start	End	Known cluster	Similarity
C1.1	NRPS,beta-lactone, transAT-PKS	1	87573	fengycin	High
C1.2	transAT-PKS,NRPS,T2PKS	152204	262297	bacillaene	High
C1.3	transAT-PKS	480988	569221	macrolactin	High
C1.4	lanthipeptide-class-ii	735784	764672	-	-
C1.5	terpene	885165	905905	-	-
C1.6	PKS-like	987949	1029193	-	-
C2.1	other	308656	350074	bacilysin	High
C2.2	NRP-metallophore,NRPS,RiPP-like	886384	938175	bacillibactin	High
C3.1	NRPS	1	38613	plipastatin	Low
C3.2	Terpene	63840	85723	-	-
C3.3	T3PKS	149041	190141	-	-
C3.4	transAT-PKS	305127	411309	difficidin	High
C3.5	terpene-precursor	434603	455493	-	-
C4.1	NRPS	1	25426	surfactin	Low
C5.1	NRPS	1	27977	surfactin	Low
C11.1	NRPS	1	9902	-	-
C12.1	NRPS	1	9529	-	-

The cell-free supernatant of B. velezensis 199 exhibits antagonistic activity and candidate amino-acid-associated metabolites

To determine whether secreted metabolites contribute to the antagonistic activity of strain 199, we compared the inhibitory effects of live strain 199 and its cell-free supernatant against *S. acidiscabies*. Compared with the 1/2 TSB control, both live strain 199 and the cell-free supernatant formed clear inhibition zones on agar plates (Fig. 3A). Quantitative analysis showed that live strain 199 exhibited the strongest inhibition, while the supernatant also significantly inhibited pathogen growth (Fig. 3B). These results indicate that the direct antagonistic activity of strain 199 is at least partly mediated by extracellular secreted metabolites.

To identify candidate metabolites associated with this extracellular antagonistic activity, we performed untargeted metabolomic profiling of cell-free supernatants from strain 199 and the non-antagonistic strain 146 (**Fig. S2A**). OPLS-DA showed a clear separation between the metabolic profiles of the strain 199 and 146 supernatants, indicating that the two strains produced distinct extracellular metabolite profiles (Fig. 3C). Consistently, volcano plot analysis identified multiple differentially accumulated metabolites in the strain 199 supernatant compared with the strain 146 supernatant (Fig. 3D). We next classified the metabolites enriched in the strain 199 supernatant. These metabolites were assigned to multiple chemical categories, including organic acids and derivatives, benzenoids, lipids and lipid-like molecules, organic oxygen compounds, phenylpropanoids and polyketides, and organic nitrogen compounds (**Fig. S2C**). Among these categories, organic acids and derivatives represented the largest group, suggesting that amino-acid-associated metabolism was a prominent feature of the extracellular metabolite profile of strain 199. Several enriched metabolites were related to amino acid metabolism, prompting us to focus on amino-acid-associated compounds as potential contributors to the bioactivity of the 199 supernatant (**Table S1**).

To identify candidate metabolites for functional evaluation, we screened the compounds detected by untargeted metabolomic profiling and prioritized three amino acids, glutamic acid, phenylalanine, and Asn, based on their practical suitability for plant-related applications. Subsequent plate, potato slice, and potato tuber assays showed that Asn exhibited comparatively favorable inhibitory or disease-suppressive activity among the tested compounds (**Fig. S2B, D**). Therefore, Asn was selected for further characterization. Targeted quantification detected Asn concentrations of approximately 9.4 and 5.8 μg/mL in the cell-free supernatants of strains 199 and 146, respectively (Fig. 3F). These results confirmed the presence of Asn in both supernatants, with a numerically higher concentration observed in strain 199 (Fig. 3E, F). Together, these results identify Asn as a candidate extracellular metabolite associated with the direct antagonistic activity of strain 199 against *S. acidiscabies*.

Biocontrol efficacy of B. velezensis 199, its cell-free supernatant, and Asn against potato common scab

To evaluate the disease-suppressive effects of strain 199, its cell-free supernatant, and Asn, we conducted greenhouse pot experiments using a planting substrate containing unsterilized natural soil that had been selected following preliminary PCR screening for potato common scab-associated pathogens. Common scab symptoms were observed even in the non-inoculated control, which may be attributable to background disease pressure associated with the use of unsterilized natural soil. This soil had been selected following preliminary PCR screening for potato common scab-associated pathogens. Under these conditions, the disease index of the water-treated control was 71.3%, whereas treatment with strain 199, its cell-free supernatant, or Asn resulted in disease indices of 56.7%, 54.0%, and 62.8%, respectively (Fig. 4A-B). After inoculation with *S. acidiscabies*, water-treated tubers developed typical common scab symptoms. In contrast, treatment with strain 199 or its cell-free supernatant visibly reduced disease symptoms on tubers (Fig. 4). Quantitative analysis showed that both strain 199 and the 199 supernatant significantly reduced disease incidence compared with the water treatment under

pathogen-inoculated conditions (Fig. 4A). Similarly, both treatments significantly decreased the disease index after *S. acidiscabies* inoculation (Fig. 4B**)**, supporting the contribution of secreted metabolites to the biocontrol activity of strain 199.

Notably, exogenous Asn also alleviated scab symptoms in pathogen-inoculated tubers (Fig. 4). Although the reduction in disease incidence by Asn was weaker than that observed for strain 199 and its cell-free supernatant, Asn significantly reduced the disease index compared with the water treatment under *S. acidiscabies* challenge (Fig. 4B). No significant differences in tuber weight-related traits were observed among treatments under pathogen-inoculated conditions (**Fig. S3A, B**).

To further assess the field performance of strain 199, we tested its biocontrol effect in three potato cultivars, including Atlantic, Favorita and Q9. In cultivar Atlantic, both strain 199 and the cell-free supernatant of strain 199 showed a trend toward reduced disease incidence and disease index without reducing tuber weight (**Fig. S4A**). In cultivars Favorita and Q9, strain 199 also tended to reduce disease incidence and disease index compared with the control (**Fig. S4B, C**). These field results provide preliminary support for the biocontrol potential of strain 199 across different potato cultivars. Together, these results suggest that strain 199 suppresses potato common scab partly through secreted metabolites, with Asn representing a candidate amino-acid-associated metabolite contributing to disease suppression.

Strain 199, its cell-free supernatant, and Asn reshape the tuber skin microbiome and enrich bacteria with antagonistic activity

To investigate the effects of strain 199, its cell-free supernatant, and Asn on the potato tuber skin microbiome, we characterized bacterial communities from tuber skin samples subjected to water control, strain 199 (B199), cell-free supernatant (B199S), or Asn treatments. The Shannon index showed no significant differences in bacterial alpha diversity between the control and any of the three treatments (**Fig. S5A**). In contrast, principal coordinate analysis (PCoA) based on Bray–Curtis dissimilarity revealed differences in bacterial community composition among treatments, with PERMANOVA indicating a significant overall treatment effect ($R^2 = 0.302$, $P = 0.001$; Fig. 5A). These results suggest that the treatments altered tuber skin bacterial community composition without significantly affecting alpha diversity.

At the phylum level, the bacterial communities were predominantly composed of Proteobacteria, Actinobacteriota, Bacteroidota, and Firmicutes (Fig. 5B). Compared with the control, B199 treatment was associated with a lower relative abundance of Proteobacteria and higher relative abundances of Bacteroidota and Actinobacteriota. B199S treatment showed higher relative abundances of Proteobacteria and Bacteroidota but a lower relative abundance of Actinobacteriota, whereas Asn treatment was associated with a lower relative abundance of Proteobacteria and a higher relative abundance of Actinobacteriota. All three treatments showed lower relative abundances of Firmicutes compared with the control. At the class level, the dominant bacterial groups included Alphaproteobacteria, Bacteroidia, Gammaproteobacteria, Actinobacteria, and Bacilli (**Fig. S5C**). These

observations indicate treatment-specific changes in the taxonomic composition of the tuber skin microbiome.

To further characterize treatment-associated community patterns, bacterial co-occurrence networks were constructed for each treatment (**Fig. S5D**). The control network contained 135 nodes and 299 edges, whereas the B199 and B199S networks contained 96 nodes and 243 edges, and 68 nodes and 122 edges, respectively. The Asn network contained 133 nodes and 459 edges. These differences indicate variation in inferred network topology among treatments, although they do not necessarily represent changes in direct microbial interactions.

To further investigate the presence of pathogen-associated bacteria in the tuber skin microbiome, we compared the representative ASV sequences with the full-length 16S rRNA gene sequence of the inoculated *Streptomyces acidiscabies* strain. Sequence alignment revealed that ASV1770 shared 98% sequence identity with the inoculated pathogen over the amplified 16S rRNA region (**Fig. S6A**). This result supports the detection of a *S. acidiscabies*-related bacterial sequence in the tuber skin microbiome, although the limited taxonomic resolution of the 16S rRNA amplicon does not allow definitive identification of the inoculated pathogen strain.

Given that strain 199, its cell-free supernatant, and Asn all reduced common scab severity under greenhouse conditions, we next investigated whether these treatments were associated with the enrichment of shared bacterial ASVs. Differential abundance analysis identified treatment-specific sets of significantly enriched ASVs relative to the control. Notably, 13 ASVs were significantly enriched across all three treatments (Fig. 5C, D). To investigate the antagonistic activity of bacteria associated with these shared enriched ASVs, we isolated culturable bacteria from potato tuber skin samples and compared their 16S rRNA gene sequences with representative ASV sequences. A bacterial isolate assigned to *Pandoraea* sp. was found to correspond to ASV1676, one of the 13 shared enriched ASVs (with 98% similarity). In plate assays, this isolate inhibited the growth of *S. acidiscabies*, producing a measurable inhibition zone, although its antagonistic activity was weaker than that of strain 199 (Fig. 5E, F). Together, the microbiome and culture-based results indicate that strain 199, its cell-free supernatant, and Asn alter the tuber skin bacterial community and are associated with the enrichment of bacteria exhibiting pathogen-inhibitory activity in vitro.

Discussion

Bacillus spp. have been widely investigated as biological control agents against potato common scab, with previous studies primarily emphasizing their direct antagonistic activity and the production of antimicrobial metabolites. However, the effects of *B. velezensis* and its extracellular products on the potato tuber skin microbiome, particularly the enrichment of bacteria with antagonistic potential, remain less well understood. In this study, we identified *B. velezensis* 199 as a promising biocontrol candidate against potato common scab. Strain 199 and its cell-free supernatant inhibited *S. acidiscabies* growth in vitro and reduced disease severity under greenhouse conditions. Metabolomic profiling and targeted

quantification identified asparagine (Asn) as a candidate extracellular metabolite in the cell-free supernatant of strain 199, while exogenous Asn independently exhibited inhibitory activity against *S. acidiscabies* and reduced common scab severity under greenhouse conditions. Furthermore, strain 199, its cell-free supernatant, and Asn altered the potato tuber skin bacterial community and were associated with the significant enrichment of 13 shared bacterial amplicon sequence variants (ASVs). Notably, a *Pandoraea* sp. isolate corresponding to one of these ASVs (ASV1676) exhibited antagonistic activity against *S. acidiscabies* in vitro. Together, these findings highlight the disease-suppressive potential of strain 199 and exogenous Asn and reveal associated changes in the tuber skin microbiome, including the enrichment of bacteria with antagonistic properties.

Asparagine is a candidate extracellular metabolite associated with Bacillus-mediated biocontrol

Previous studies have established that the biocontrol activity of *Bacillus* spp. is primarily attributed to secondary metabolites such as surfactin, fengycin, and bacillaene (Saiyam et al. 2024; Balleux et al. 2025). These lipopeptides and polyketides suppress pathogens through membrane disruption, inhibition of cell wall synthesis, or induction of plant systemic resistance, and therefore have become the major focus of research on *Bacillus*-mediated biological control (Ongena and Jacques 2008; Maksimov et al. 2020). Consistent with these reports, genome mining of strain 199 revealed multiple biosynthetic gene clusters encoding these classical antimicrobial compounds, suggesting that strain 199 possesses the genetic capacity to synthesize diverse bioactive metabolites (Fig. 2).

In addition to these predicted antimicrobial metabolites, our untargeted metabolomic analysis highlighted Asn as a candidate amino-acid-associated metabolite enriched in the extracellular metabolite profile of strain 199. Metabolomic profiling showed that Asn was more abundant in the cell-free supernatant of strain 199 than in that of the non-antagonistic strain 146, and targeted quantification further supported its enrichment in strain 199 (Fig. 3). Moreover, exogenous Asn inhibited the growth of *S. acidiscabies* in vitro and reduced potato common scab severity under greenhouse conditions, indicating that amino-acid-associated metabolites may contribute to the disease-suppressive activity of strain 199 (Fig. 4). However, Asn should be interpreted as a candidate contributor rather than the sole active compound responsible for the antagonistic activity of the cell-free supernatant. Asn itself has rarely been reported to function as a direct antimicrobial compound. Instead, it occupies a central position in nitrogen metabolism by linking carbon and nitrogen fluxes and providing substrates for amino acid and protein biosynthesis (Gaufichon et al. 2010; Qiao et al. 2026). Therefore, one possibility is that Asn functions as a metabolic precursor supporting the biosynthesis of peptide-derived secondary metabolites or other bioactive compounds secreted by strain 199 (Aoki et al. 2025). Another, non-mutually exclusive possibility is that Asn modifies nutrient availability in the tuber skin microenvironment, thereby altering microbial interactions and favoring the enrichment of antagonistic core microorganisms (Shafi and Shahid 2025; Ma et al. 2026). This interpretation could explain the observation that Asn treatment was associated with changes in tuber skin microbiome and shared a common set of enriched ASVs with strain 199 and its cell-free supernatant. Further studies using targeted metabolomics, dose-response assays, metabolite depletion or complementation, and SynCom-

based tuber or pot experiments will be needed to clarify the relative contribution of Asn to direct antagonism and microbiome-mediated disease suppression.

Host genotype may influence the field performance of strain 199

Although strain 199 consistently suppressed potato common scab under greenhouse conditions, its field performance varied among potato cultivars (Fig. 4, Fig.S4). In the present study, strain 199 showed a tendency to reduce disease incidence and/or disease index in Atlantic, Favorita, and Q9, but the magnitude of disease suppression differed among cultivars. This cultivar-dependent pattern suggests that the interaction between strain 199, the host plant, and the indigenous microbiota may influence biocontrol outcomes under field conditions (Chen et al. 2021). These observations indicate that successful biological control depends not only on the intrinsic antagonistic capacity of the introduced strain but also on its establishment, activity, and ecological compatibility within the host-associated niche. Host genotype is now recognized as one of the major factors shaping plant-associated microbial communities (Zhang et al. 2023). Different potato cultivars differ in root exudate composition, tuber metabolites, and immune responses, all of which influence microbial colonization and persistence (Aversano et al. 2017; Asakaviciute et al. 2025; Zhang et al. 2026). These host-dependent characteristics determine not only the assembly of indigenous microbiota but also the establishment of introduced beneficial microorganisms. Previous studies have demonstrated that potato cultivars harbor distinct rhizosphere and tuber-associated microbial communities, which consequently influence the performance of microbial inoculants (Buchholz et al. 2019; Zhao et al. 2025). Therefore, the cultivar-dependent field performance observed in this study may be associated with differences in host-associated niches that influence the persistence of strain 199, the activity of its secreted metabolites, and the assembly of suppressive microbial communities. Future studies comparing root exudates, tuber skin metabolites, strain 199 colonization, and microbiome assembly among potato cultivars will help clarify how host genotype regulates the interaction between strain 199, the indigenous microbiota, and the potato common scab pathogen.

Enrichment of antagonistic bacteria in the tuber skin microbiome following disease-suppressive treatments

Beyond their direct antagonistic activity against *S. acidiscabies*, *B. velezensis* 199, its cell-free supernatant, and exogenous Asn induced distinct changes in the potato tuber skin bacterial community (Fig. 5A,B). Notably, differential abundance analysis identified 13 ASVs that were significantly enriched across all three treatments compared with the control (Fig. 5C, D). Although the treatments differed in their overall effects on bacterial community composition, the shared enrichment of these ASVs suggests a common microbiome response associated with disease suppression. Previous studies have demonstrated that plant-associated microbial communities can contribute to pathogen suppression through microbial competition and the activity of beneficial microorganisms (Shi et al. 2019; Carrión et al. 2019; Zhou et al. 2022; Zhou et al. 2025). In this study, the 13 shared enriched ASVs may represent a

group of treatment-responsive bacteria worthy of further investigation for their potential roles in potato common scab suppression.

Importantly, the biological relevance of these shared enriched ASVs was further explored through the isolation and functional characterization of a culturable representative. Although its inhibitory activity was weaker than that of strain 199, the ability of this isolate to inhibit pathogen growth provides initial functional evidence that the shared enriched bacterial community contains microorganisms with antagonistic properties. Additionally, previous studies have shown that certain *Pandoraea* strains can produce antibacterial compounds and suppress plant pathogen infection, thereby contributing to plant protection (Wu et al. 2019; Jin et al. 2007). Nevertheless, the enrichment of ASV1676 and the antagonistic activity of its corresponding isolate do not establish a causal contribution to disease suppression in planta. Further studies assessing its colonization, persistence, and disease-suppressive activity under greenhouse conditions will be required to clarify its ecological role.

The shared enrichment of ASV1676 following treatment with strain 199, its cell-free supernatant, and Asn is particularly interesting. Although the three treatments differ in composition and biological activity, they may influence aspects of the tuber-associated environment that favor certain bacterial populations. Asn, an amino acid involved in nitrogen metabolism, may alter nutrient availability and thereby influence bacterial community composition (Liu et al. 2020; Zeng et al. 2016; Gaufichon et al. 2010). However, the present results do not establish whether Asn directly promotes the enrichment of ASV1676 or whether the Asn present in the supernatant of strain 199 mediates the observed microbiome changes. The overlap in enriched ASVs should therefore be interpreted as evidence of a shared treatment-associated microbial response rather than a demonstrated metabolite-driven recruitment mechanism. Further experiments involving Asn depletion and complementation, together with assays examining the growth and colonization responses of the *Pandoraea* isolate to Asn, would help clarify these relationships.

The detection of ASV1770, which showed 98% sequence identity to the inoculated *S. acidiscabies* strain within the amplified 16S rRNA region, further indicated the presence of pathogen-related *Streptomyces* sequences in the tuber skin microbiome. However, the limited resolution of 16S rRNA amplicon sequencing prevents definitive identification of pathogenic *Streptomyces* species or differentiation of the inoculated strain from closely related indigenous bacteria. Moreover, changes in the relative abundance of this ASV cannot directly establish changes in pathogen population size or virulence. Therefore, further pathogen-specific quantitative analyses would be required to determine whether the treatments affect pathogen colonization or abundance.

Collectively, our findings indicate that the disease-suppressive effects of strain 199, its cell-free supernatant, and exogenous Asn are accompanied by changes in the potato tuber skin microbiome and the enrichment of a shared set of bacterial ASVs. The identification of an antagonistic *Pandoraea* sp. isolate corresponding to ASV1676 provides preliminary functional support for the presence of pathogen-inhibitory bacteria among these enriched microorganisms. These observations suggest that treatment-

associated microbiome changes may represent an additional ecological feature of PCS biocontrol, although their direct contribution to disease suppression remains to be established.

Conclusion

In conclusion, this study identified *Bacillus velezensis* 199 as a promising biocontrol candidate against potato common scab. Strain 199 and its cell-free supernatant inhibited *Streptomyces acidiscabies* growth in vitro and reduced disease severity under greenhouse conditions, while field trials provided preliminary evidence of its biocontrol potential. Metabolomic analysis identified asparagine (Asn) as a candidate extracellular metabolite in the cell-free supernatant of strain 199, and exogenous Asn independently exhibited inhibitory activity against *S. acidiscabies* and reduced common scab severity under greenhouse conditions. Furthermore, strain 199, its cell-free supernatant, and Asn altered the potato tuber skin bacterial community and were associated with the significant enrichment of 13 shared bacterial amplicon sequence variants (ASVs). A *Pandoraea* sp. isolate corresponding to one of these ASVs (ASV1676) exhibited antagonistic activity against *S. acidiscabies* in vitro. Collectively, these findings highlight the disease-suppressive potential of strain 199 and exogenous Asn and reveal associated changes in the tuber skin microbiome, including the enrichment of an ASV closely matching an antagonistic bacterial isolate. Further investigations are needed to determine the contribution of Asn to the activity of strain 199 and establish whether the enriched bacterial taxa participate in disease suppression in planta.

Methods

Selection of antagonistic bacteria

Modified Gauze's Medium No. 1 (GM; Coolaber Co., MM5030-250g) agar plates were prepared for the screening of antagonistic bacteria. Four wells were made in each GM agar plate and filled with TSA medium. The pathogenic *S. acidiscabies* strain was cultured on GM for 5 days and then transferred to TSB medium at 28°C with shaking at 200 rpm for 3 days. The resulting *S. acidiscabies* suspension was evenly spread onto the modified GM agar plates. *Bacillus* isolates maintained in our laboratory were cultured at 28℃ in a rotary shaker with 200 rpm in 1/2 TSB liquid media for 12 hours and the washed with 10 mM $MgSO_4$ to remove 1/2 TSB media. The bacterial suspensions were adjusted at OD_{600} = 1 and inoculated with 2 µL on the modified GM media plates for 5 days. Bacteria that caused the largest inhibited circle were considered antagonistic strains.

Pot assay

Before preparation of the planting substrate, natural soil samples were screened for potato common scab-associated pathogens using pathogen-targeting PCR primers (F: GACGTCCCGGGCGAACTCCTG, R: GGCCGCCCACCGTAACTGCTCAC). Soil samples yielding the expected amplification product were

selected and incorporated into the planting substrate. The selected natural soil was not sterilized before use. Consequently, the planting substrate potentially contained indigenous pathogenic *Streptomyces* populations, providing a background of naturally occurring disease pressure during the greenhouse experiments.

The *S. acidiscabies* strain were inoculated into 1/2 TSB and incubated at 28 ℃ in a rotary shaker (200 rpm) for 3 days. The bacterial cells were collected and adjusted to final concentration of 1×10^8 CFU/mL for preparation.

Seed tubers of *Solanum tuberosum* L. cv. Atlantic were planted at a depth of 5–6 cm. At the tuber emergence, flowering, and tuber formation stages, 100 mL of the corresponding inoculation suspension or treatment solution was applied near the roots of each plant. For strain 199 treatment, strain 199 was cultivated for 12 hours on 1/2 TSB medium at 28 ℃ and 200 rpm to OD_{600} = 1. 100 mL containing 10^8 CFU were applied to the treatments. For metabolite treatment, Asn were dissolved in water with a final concentration of 1 ppm. Each of the nine treatments included for potato tubers: (a) control: without treatments or *S. acidiscabies*; (b) water: *S. acidiscabies* only; (c) treatment only; (d) treatment and *S. acidiscabies.* Potato plants were watered twice weekly at early stage and every day at flowering and tuber stage with 500 mL water, and fertilizer (20-20-20, PUREY China) was applied weekly after potato seedlings emerged. At 120 days after seed tubers were planted, the tubers were harvested and assessed for PCS.

Field trial

A field trial with a randomized block design was set up in Dapeng County (22°59′N, 114°50′E), Shenzhen city, Guangdong Province, China. Potatoes have been continuously grown at this site for 5 years, and plantings had a high percentage of PCS in the past year across various cultivars. Three cultivars were selected including *Solanum tuberosum* L. cv. Atlantic, *Solanum tuberosum* L. cv. Favorita and *Solanum tuberosum* L. cv. Q9. For *Solanum tuberosum* L. cv. Favorita and *Solanum tuberosum* L. cv. Q9, the site was divided into two groups: (a) the control, which was not inoculated with the strain 199, and (b) the treatment which was inoculated with strain 199. For *Solanum tuberosum* L. cv. Atlantic, (c) an additional treatment with the cell-free supernatant of strain 199 was included. At the flowering stage, 100 mL of strain 199 suspension (1×10^6 CFU/mL) or the cell-free supernatant of strain 199 was applied to each plant according to the treatment design. Tuber seeds were sown in the soil on December 2nd, 2025 and the soil was then covered with plastic film until harvest. At period of flowering stage, the strain 199 and its supernatant were inoculated. Potatoes were harvested on March 22, 2026.

Disease assessment

The disease rate was calculated using following equation:

Disease rate = (number of infected tubers / total number of tubers) × 100% (1)

The disease index was calculated as previous described(Tao et al. 2023):

Disease index = $[\sum(n_i \times i) / (N \times 5)] \times 100$ (2)

Where i represents the disease severity score from 0 to 5 based on the percentages of tubers covered by lesions (0: no lesions, 1: 0–12.5%, 2: 12.6% – 25%, 3: 26% – 50%, 4: 51–75%, and 5: 76–100%, respectively), n_i is the number of tubers assigned to score i, and N is the total number of tubers assessed.

Metabolomics analysis

Single colonies were picked from agar plates and inoculated into 50 mL of 1/2 tryptic soy broth (1/2 TSB), followed by incubation at 25°C for 24 h with shaking at 200 rpm. The cultures were then evenly aliquoted into 10 mL centrifuge tubes, and the cell density was adjusted to an OD600 of 1.0. After centrifugation at 4,000 rpm for 5 min, the supernatants were collected and filtered through 0.22 μm filters to ensure the complete removal of viable cells. The resulting cell-free culture supernatants were subsequently lyophilized to obtain dried metabolite extracts.

For metabolite extraction, an appropriate amount of lyophilized sample was accurately weighed and transferred into a 2 mL centrifuge tube. Then, 300 μL of internal standard solution, containing 2-chloro-L-phenylalanine at 4 ppm in 80% aqueous methanol, was added to each sample. The mixture was vortexed for 1 min and centrifuged at 12,000 rpm for 10 min at 4°C. The supernatant was collected, filtered through a 0.22 μm microporous membrane, and transferred into LC-MS vials for subsequent analysis.

Chromatographic separation was performed using a Thermo Vanquish ultra-high-performance liquid chromatography system equipped with an ACQUITY UPLC® HSS T3 column (2.1 × 100 mm, 1.8 μm). The column temperature was maintained at 40°C, the flow rate was set to 0.3 mL/min, and the injection volume was 5 μL. For analysis in positive ion mode, mobile phase A consisted of water containing 0.1% formic acid, while mobile phase B consisted of acetonitrile containing 0.1% formic acid. The gradient elution program was as follows: 0–1 min, 10% B; 1–5 min, 10–98% B; 5–6.5 min, 98% B; 6.5–6.6 min, 98–10% B; and 6.6–8 min, 10% B. For negative ion mode, mobile phase A was 5 mM ammonium formate in water, and mobile phase B was acetonitrile. The same gradient program was applied for negative ion mode analysis.

Mass spectrometric detection was carried out using a Thermo Orbitrap Exploris 120 mass spectrometer equipped with an electrospray ionization source. Data were acquired separately in both positive and negative ion modes. The spray voltage was set to 3.50 kV for positive ion mode and − 2.50 kV for negative ion mode. The sheath gas and auxiliary gas flow rates were set to 40 arb and 10 arb, respectively, and the capillary temperature was maintained at 325°C. Full-scan MS data were acquired at a resolution of 60,000 over an m/z range of 100–1000. Data-dependent acquisition was employed for MS/MS analysis, in which the top four most intense precursor ions were selected for fragmentation. The

normalized collision energy was set to 30%, the MS/MS resolution was 15,000, and dynamic exclusion was enabled to avoid repeated acquisition of the same ions.

Raw LC-MS data were converted into an appropriate format and processed using metabolomics data analysis software for peak detection, alignment, correction, and deconvolution. A data matrix containing mass-to-charge ratio, retention time, and peak area was generated for downstream analysis. Metabolite annotation was performed by matching accurate mass measurements with a mass error threshold of ≤ 5 ppm and comparing MS/MS fragmentation spectra against public databases, including HMDB, METLIN, and KEGG, as well as an in-house standard compound database.

Asparaginase activity assay

Asparaginase (ASNase) activity was determined using an asparaginase activity assay kit (Cat# BC1600) according to the manufacturer's instructions with minor modifications. Briefly, single colonies of strains 199 and 146 were picked from 1/2 TSA plates and inoculated into 1/2-strength TSB medium in 50 mL centrifuge tubes. The cultures were incubated at 28°C with shaking at 200 rpm for 24 h, and the cell density was adjusted to an OD_{600} of 1.0. For intracellular enzyme extraction, bacterial suspensions were mixed with extraction buffer at a ratio corresponding to 1 × 10^6 cells per 1 mL extraction buffer. The mixtures were disrupted by ultrasonic treatment on ice at 200 W, with 3 s sonication and 7 s intervals for a total duration of 3 min. The lysates were centrifuged at 4,000 × g for 10 min at 4°C, and the supernatants were collected and kept on ice for subsequent analysis. For extracellular enzyme activity detection, bacterial cultures were filtered through 0.22 μm membranes to remove viable cells, and the resulting cell-free filtrates were directly used for the assay.

For the enzymatic reaction, 200 μL of each sample was mixed with 200 μL of reagent I in the assay tube, whereas the control tube contained 200 μL of sample without reagent I during the initial reaction. The mixtures were incubated at 37°C for 6 h. After the enzymatic reaction, 400 μL of reagent II was added to both assay and control tubes and mixed thoroughly for 1 min. Then, 200 μL of reagent I was added to the control tube. The mixtures were centrifuged at 10,000 × g for 10 min at 4°C. Subsequently, 400 μL of supernatant from each assay or control tube was transferred to a new 1.5 mL tube and mixed with 400 μL each of reagent III and reagent IV. For the standard and blank reactions, 400 μL of 300 nmol/mL ammonia standard or distilled water was mixed with reagent III and reagent IV, respectively. All reactions were incubated at 37°C for 20 min.

After incubation, 1 mL of the reaction mixture was transferred into a glass cuvette, and the absorbance at 630 nm was measured. The absorbance values of the assay tube, control tube, standard tube, and blank tube were recorded as A_assay, A_control, A_standard, and A_blank, respectively. The absorbance differences were calculated as ΔA_assay = A_assay − A_control and ΔA_standard = A_standard − A_blank. ASNase activity was calculated according to the kit instructions. For cell-based normalization, ASNase activity was expressed as U/10^6 cells using the following equation:

ASNase activity (U/10^6 cells) = 200 × ΔA_assay / ΔA_standard / N × F

For volume-based normalization, ASNase activity was expressed as U/mL using the following equation:

ASNase activity (U/mL) = 200 × ΔA_assay / ΔA_standard × F

where N represents the total number of cells in millions, and F represents the dilution factor.

Asparagine content assay

The L-asparagine (Asn) content of *Bacillus velezensis* 199 and the non-antagonistic strain 146 was determined using a commercial L-asparagine assay kit according to the manufacturer's instructions, with minor modifications. Single colonies of strains 199 and 146 were picked from half-strength tryptic soy agar (1/2 TSA) plates and inoculated into 3 mL of tryptic soy broth (TSB) in 12 mL centrifuge tubes. The cultures were incubated at 28°C with shaking at 200 rpm for 24 h, and the cell density was subsequently adjusted to an optical density at 600 nm (OD600) of 1.0. For extracellular Asn extraction, bacterial cultures adjusted to an OD600 of 1.0 were passed through 0.22 μm filters to remove cells. The resulting cell-free supernatants (0.8 mL) were mixed with an equal volume of chloroform, vortexed for 5 min, and centrifuged at 10,000 × g for 10 min at 4°C. The upper aqueous phase was collected and maintained on ice for subsequent quantification. Asn content was determined using a 96-well UV-transparent microplate. For each sample, the reaction well contained 20 μL of sample extract, 60 μL of reagent II-B, and 10 μL of reagent III, whereas the corresponding control well contained 20 μL of sample extract and 70 μL of reagent II-B. After mixing, the reaction mixtures were incubated at 37°C for 5 min. Subsequently, 100 μL of freshly prepared working solution, consisting of reagents I and II at a volume ratio of 4:1, was added to each well, and the initial absorbance (A1) was measured at 340 nm. Reagent IV (10 μL) was then added to both the reaction and control wells, followed by incubation at 37°C for 10 min. The final absorbance (A2) was measured at 340 nm within 5 min after incubation.

The absorbance difference (ΔA) was calculated as follows:

ΔA = (A1, reaction − A2, reaction) − (A1, control − A2, control).

For extracellular samples, Asn content was expressed as μg/mL and calculated using the following equation:

Asn content (μg/mL) = 353.97 × ΔA × F.

where F represents the sample dilution factor.

Tuber skin sampling and preparation

Healthy potato tubers were selected as experimental materials. Potato tuber skin samples were aseptically collected using sterile tools. For each sample, an appropriate amount of tuber skin tissue was scraped from the tuber surface and transferred into a sterile centrifuge tube for subsequent amplicon sequencing and microbial isolation. All sampling tools were autoclaved or disinfected with 75% ethanol before use.

Selection and functional screening of candidate metabolites

Following untargeted metabolomic profiling of the cell-free supernatants of *B. velezensis* 199 and the non-antagonistic strain 146, annotated metabolites were screened to identify candidates for functional evaluation. Metabolite derivatives were excluded, and compounds with relatively low cost and suitability for plant-related applications were prioritized. Based on these criteria, three amino acids, phenylalanine (Phe), glutamic acid (Glu), and asparagine (Asn), were selected for subsequent screening.

For the plate assay, each amino acid was dissolved separately in sterile distilled water and added to sterilized potato dextrose agar (PDA) medium at a final concentration of 1 ppm before plate pouring. PDA supplemented with an equivalent volume of sterile distilled water served as the control. After solidification, 100 µL of *Streptomyces acidiscabies* suspension (1×10^6 CFU/mL) was evenly spread onto each plate. The plates were incubated at 28°C, and pathogen growth was evaluated relative to the control.

For the potato slice assay, healthy tubers of the potato cultivar Atlantic were cut into pieces. Each amino acid solution (1 ppm) was uniformly sprayed onto the potato tissue surface and allowed to air-dry before pathogen inoculation. Three inoculation sites were established on each potato piece, and one *S. acidiscabies* colony collected from an agar plate using a sterile pipette tip was placed at each inoculation site.

For the potato peel assay, peel tissues were excised from healthy Atlantic potato tubers. Each amino acid solution (1 ppm) was uniformly sprayed onto the peel surface and allowed to air-dry. Three inoculation sites were established on each peel sample, and one *S. acidiscabies* colony was transferred to each site using a sterile pipette tip.

The inoculated potato tissues were incubated at 28°C for 5 days, after which pathogen growth and lesion development were evaluated. Three independent potato tubers were used as biological replicates for each treatment (n = 3). Based on the comparative screening results, Asn was selected for subsequent investigation.

Isolation and cultivation of tuber skin microorganisms

To isolate culturable microorganisms associated with the potato tuber skin, five tubers from each treatment, including strain 199, the cell-free supernatant of strain 199 and asparagine, were randomly selected after harvest. The tuber skin was aseptically scraped using a sterile measuring spoon, and the skin tissues from the five tubers within each treatment were pooled and suspended in sterile 0.9% (w/v) NaCl solution. The suspension was vortexed vigorously for 2 min to detach microorganisms from the tuber surface. Serial ten-fold dilutions (10^{-1}, 10^{-2}, and 10^{-3}) were prepared, and 100 µL of each dilution was spread onto potato dextrose agar (PDA) and 1/5 tryptic soy agar (1/5 TSA) plates. The plates were incubated at 28°C for 5 days. Colonies with distinct morphologies were selected daily throughout the

incubation period and purified by repeated streaking on the corresponding medium to obtain pure isolates for subsequent characterization.

Amplicon sequencing and bioinformatic analysis of tuber skin bacteria

Tuber skin samples were collected for bacterial community analysis. Total microbial DNA was extracted using the DNeasy PowerSoil Pro Kit (Qiagen, Hilden, Germany) according to the manufacturer's instructions. The concentration and quality of the extracted DNA were assessed prior to PCR amplification. The V4–V5 hypervariable region of the bacterial 16S rRNA gene was amplified using the primer pair 515F (5'-GTGCCAGCMGCCGCGGTAA-3') and 944R (5'- CCGTCAATTCCTTTGAGTTT-3'). PCR amplification was performed using the extracted DNA as the template. The PCR products were examined for quality and then submitted to Novogene Co., Ltd. (Beijing, China) for high-throughput sequencing on the Illumina HiSeq platform.

Raw sequencing data were first subjected to quality control to remove low-quality reads, adaptor sequences, and ambiguous sequences, resulting in high-quality clean reads. Subsequent bioinformatic analyses were performed using QIIME2 software (v2024.2)(Bolyen et al. 2019). Paired-end reads were quality-filtered, trimmed, merged, and denoised using the DADA2(Callahan et al. 2016) algorithm to generate amplicon sequence variants (ASVs). Taxonomic classification of bacterial ASVs was conducted using naïve Bayes classifier against the SILVA 138.1 database (Quast et al. 2013).

The resulting ASV table and taxonomic annotation table were used for downstream microbial community analyses, including community composition profiling, alpha-diversity analysis, beta-diversity analysis, and comparative analysis of bacterial community structure among control tuber skin sample (Control), strain 199-treated tuber skin sample (B199), 199-supernatant tuber skin sample (B199S) and Asn-treated tuber skin sample (Asn).

Differential abundance analysis of bacterial amplicon sequence variants (ASVs) was performed using DESeq2 based on the ASV count table. Each treatment (B199, B199S, or Asn) was compared separately with the control. *P* values were adjusted for multiple testing using the Benjamini–Hochberg procedure. ASVs with an adjusted *P* value below 0.05 and a positive $\log_2$ fold change > 1 were considered significantly enriched. Shared enriched ASVs were defined as those meeting these criteria in all three treatment-versus-control comparisons.

Phylogenetic Analysis and Taxonomic Identification

To determine the exact taxonomic position of strain 199 within the genus Bacillus, phylogenomic and genomic similarity analyses were performed. The proteome and genome sequences of strain 199 along with closely related reference strains were utilized. Orthologous groups were identified using OrthoFinder. Briefly, a multiple sequence alignment (MSA) strategy (-M msa) was executed, where single-copy orthologous proteins were aligned using MAFFT (-A mafft), and a maximum-likelihood species tree was subsequently inferred using FastTree (-T fasttree). To further evaluate genomic relatedness at the

nucleotide level, the Average Nucleotide Identity (ANI) was calculated using FastANI based on the whole-genome sequences. Finally, the resulting phylogenetic tree and the corresponding ANI matrix were visualized and refined using the ChiPlot online platform (https://www.chiplot.online/).

Identification of culturable isolates corresponding to core ASVs

To determine whether the culturable isolates corresponded to the shared enriched ASVs identified by amplicon sequencing, the 16S rRNA gene sequences of selected isolates were compared with representative ASV sequences. Pairwise sequence alignments were performed between selected core ASVs and their corresponding isolates by using DNAMAN. Isolates showing identical or highly similar 16S rRNA sequences to the target ASVs were considered culturable representatives of the corresponding ASVs. In addition, ASV1770 showed 98% sequence similarity to the inoculated *S. acidiscabies* strain and was therefore defined as a *S. acidiscabies*-like ASV.

Statistical analysis

All experiments were performed with defined biological replicates: plate confrontation assays were conducted with three independent biological replicates; pot experiments included five biological replicates for treatments without pathogen inoculation and nine biological replicates for treatments with pathogen inoculation. Data are presented as the mean ± standard error of the mean (SEM). Statistical analyses were conducted using R software (version 4.2.2). Differences between two groups were assessed using Student's *t*-test. For experiments involving both pathogen inoculation and microbial or metabolite treatments, two-way ANOVA was used to evaluate the effects of pathogen inoculation, treatment, and their interaction. When treatments were compared with the corresponding water control within the same inoculation condition, Dunnett’s multiple comparison test was used. Statistical significance was defined as $P < 0.05$.

For microbiome analyses, alpha diversity indices (Shannon and Chao1) were calculated in R, and beta diversity was evaluated by principal coordinate analysis (PCoA) based on Bray-Curtis dissimilarity. Differences in bacterial community composition were assessed using permutational multivariate analysis of variance (PERMANOVA) with 999 permutations. Relative abundances of bacterial taxa were calculated after normalization to the total sequence counts of each sample. Differential abundance at the phylum and class levels was evaluated by comparing the mean relative abundance of each treatment with the control using Student's t-test followed by Benjamini–Hochberg (BH) correction for multiple testing. For ASV-level analysis, the $\log_2$ fold change ($\log_2$FC) of each treatment relative to the control was calculated after adding a pseudocount (1×10^{-6}). ASVs with $\log_2\text{FC} > 0$ were defined as enriched ASVs, and the intersection of enriched ASVs among the B199, B199S, and Asn treatments was designated as the shared core ASVs. Heatmaps and Venn diagrams were generated using the ComplexHeatmap and VennDiagram packages in R, respectively.

Abbreviations

ANI
Average nucleotide identity
Asn
Asparagine
ASVs
Amplicon sequence variants
BH
Benjamini-Hochberg
CDSs
Coding sequences
COGs
Clusters of Orthologous Groups of proteins
Glu
glutamic acid
LC-MS
Liquid Chromatograph-Mass Spectrometer
OPLS-DA
Orthogonal partial least-squares discriminant analysis
PCoA
Principal coordinate analysis
PCS
Potato common scab
PDA
potato dextrose agar
PERMANOVA
permutational multivariate analysis of variance
PGPRs
Plant growth-promoting rhizobacteria
Phe
phenylalanine
SEM
Standard error of the mean
TSA
tryptic soy agar

Declarations

Ethics declarations

Ethics approval and consent to participate

Not applicable.

Consent for publication

Not applicable.

Competing interests

The authors declare no competing interests.

Author information

Yuxiao Zeng: zengyx1223@sina.com

Subinur Emer: 3365104370@qq.com

Bo Zhang: zhangbo06@caas.cn

Tao Yang: youngtao1015@163.com

Qian Tao: taoq0420@163.com

Shuai Luo: law_seo@163.com

Jialin Rao: rao_jialin@webmail.hzau.edu.cn

Xingyao Xiong: xiongxingyao@caas.cn

Corresponding author

Correspondence to Yunyue Wang and Xu Cheng

Funding

Yuelushan Laboratory Talent Program (2025RC3001)

Author Contribution

WYY and CX conceived and designed the study. ZYX and SE performed the experiments. ZB screened candidate metabolites. RJL and LS analyzed the data of bacterial genome and amplicon sequence. TQ and YT coordinated the greenhouse and field experiments. ZYX wrote the original draft of the manuscript. XXY supervised the whole study processes, and reviewed the manuscript. CX and ZYX

revised the manuscript. All authors discussed the results, contributed to data interpretation, and approved the final version of the manuscript.

Acknowledgement

We acknowledge Yanli Yang from Yunnan Agricultural University support Streptomyces acidiscabies.

Data Availability

The raw sequencing reads are available from National Center for Biotechnology Information (NCBI) database with the accession numbers PRJNA1497619. The processed ASV tables and custom R scripts are also available upon request.

References

1. Aoki R, Kumagawa E, Kamata K, Ago H, Sakai N, Hasunuma T, Taoka N, Ohta Y, Kobayashi S (2025) Engineering of acyl ligase domain in non-ribosomal peptide synthetases to change fatty acid moieties of lipopeptides. Commun Chem, 8
2. Asakaviciute R, Zelya A, Andriychuk T, Razukas A (2025) Evaluation of Potato Varieties for Yield, Quality, and Late Blight Resistance. Life-Basel, 15
3. Aversano R, Contaldi F, Adelfi MG, D'amelia V, Diretto G, De Tommasi N, Vaccaro C, Vassallo A, Carputo D (2017) Comparative metabolite and genome analysis of tuber-bearing potato species. Phytochemistry 137:42–51
4. Balleux G, Hofte M, Arguelles-Arias A, Deleu M, Ongena M (2025) Bacillus lipopeptides as key players in rhizosphere chemical ecology. Trends Microbiol 33:80–95
5. Berendsen RL, Pieterse CM, Bakker PA (2012) The rhizosphere microbiome and plant health. Trends Plant Sci 17:478–486
6. Biessy A, Filion M (2022) Biological control of potato common scab by plant-beneficial bacteria. Biol Control, 165
7. Bolyen E, Rideout JR, Dillon MR, Bokulich NA, Abnet CC, Al-Ghalith GA, Alexander H, Alm EJ, Arumugam M, Asnicar F, Bai Y, Bisanz JE, Bittinger K, Brejnrod A, Brislawn CJ, Brown CT, Callahan BJ, Caraballo-Rodríguez AM, Chase J, Cope EK et al (2019) vol 37, pg 852,. 2019. Reproducible, interactive, scalable and extensible microbiome data science using QIIME 2 Nature Biotechnology, 37, 1091–1091
8. Buchholz F, Antonielli L, Kostic T, Sessitsch A, Mitter B (2019) The bacterial community in potato is recruited from soil and partly inherited across generations. PLoS ONE, 14
9. Callahan BJ, Mcmurdie PJ, Rosen MJ, Han AW, Johnson AJA, Holmes SP (2016) DADA2: High-resolution sample inference from Illumina amplicon data. Nat Methods 13:581–

10. Cao JJ, Ma Y, Fu J, Wang ZQ, Zhao YL, Zhong NQ, Zhao P (2025) DX-9 biocontrol against potato common scab involves significant changes in the soil microbiome and metabolome. Abiotech 6:33–49
11. Carrión VJ, Perez-Jaramillo J, Cordovez V, Tracanna V, De Hollander M, Ruiz-Buck D, Mendes LW, Van Ijcken WFJ, Gomez-Exposito R, Elsayed SS, Mohanraju P, Arifah A, Van Der Oost J, Paulson JN, Mendes R, Van Wezel GP, Medema MH, Raaijmakers JM (2019) Pathogen-induced activation of disease-suppressive functions in the endophytic root microbiome. Science 366:606–
12. Chen QL, Hu HW, He ZY, Cui L, Zhu YG, He JZ (2021) Potential of indigenous crop microbiomes for sustainable agriculture. Nat Food 2:233–240
13. Dahal K, Li XQ, Tai H, Creelman A, Bizimungu B (2019) Improving Potato Stress Tolerance and Tuber Yield Under a Climate Change Scenario - A Current Overview. Front Plant Sci, 10
14. Dees MW, Wanner LA (2012) In Search of Better Management of Potato Common Scab. Potato Res 55:249–268
15. Devaux A, Kromann P, Ortiz O (2014) Potatoes for Sustainable Global Food Security. Potato Res 57:185–199
16. Doumbou CL, Akimov VV, Beaulieu C (1998) Selection and characterization of microorganisms utilizing thaxtomin A, a phytotoxin produced by streptomyces scabies. Appl Environ Microbiol 64:4313–4316
17. Gaufichon L, Reisdorf-Cren M, Rothstein SJ, Chardon F, Suzuki A (2010) Biological functions of asparagine synthetase in plants. Plant Sci 179:141–153
18. He SD, Li LL, Lv MH, Wang RX, Wang LJ, Yu SW, Gao Z, Li X (2024) PGPR: Key to Enhancing Crop Productivity and Achieving Sustainable Agriculture. Current Microbiology, 81
19. Hill J, Lazarovits G (2005) A mail survey of growers to estimate potato common scab prevalence and economic loss in Canada. Can J Plant Pathol 27:46–52
20. Jiang Y, He PF, Kong HH, He PB, Wu YX, Tang GW, Tang P, Di YN, Li XY, Liu LF, Munir S, He YQ (2025) Biocontrol Effect of D7-8 on Potato Common Scab and Its Complete Genome Sequence Analysis, vol 13. Microorganisms
21. Jin ZX, Wang C, Chen W, Chen X, Li X (2007) Induction of oxalate decarboxylase by oxalate in a newly isolated Pandoraea sp. OXJ-11 and its ability to protect against Sclerotinia sclerotiorum infection. Can J Microbiol 53:1316–1322
22. Liu MS, Zhang WH, Wang XG, Wang FH, Dong WX, Hu CS, Liu BB, Sun RB (2020) Nitrogen leaching greatly impacts bacterial community and denitrifiers abundance in subsoil under long-term fertilization, vol 294. Agriculture Ecosystems & Environment
23. Liu N, Lv M, Wang Y, Ma H, Fan W, Ma J, Wang J, Gao Y, Ma J, Zhou B, Shi W, Gao Z (2026) Inhibition of potato common scab by Bacillus subtilis XT11 and its reshaping of the microbial community in potato geocaulosphere soil. World J Microbiol Biotechnol, 42
24. Loria R, Kers J, Joshi M (2006) Evolution of plant pathogenicity in Streptomyces. Annu Rev Phytopathol 44:469–487

25. Ma A, Xun W, Zhang S, Liang S, Wei W, Huang H, Shen Q, Xu G, Zhang R (2026) Amino-acid-transporter-mediated assembly of rhizosphere microbiota enhances soil organic nitrogen acquisition in rice. Nat Plants 12:356–368
26. Majeed A, Muhammad Z (2020) An overview of the common bacterial diseases of potato in Pakistan, associated crop losses and control stratagems. J Plant Pathol 102:3–10
27. Maksimov IV, Singh BP, Cherepanova EA, Burkhanova GF, Khairullin RM (2020) Prospects and Applications of Lipopeptide-Producing Bacteria for Plant Protection (Review). Appl Biochem Microbiol 56:15–28
28. Ongena M, Jacques P (2008) lipopeptides:: versatile weapons for plant disease biocontrol. Trends Microbiol 16:115–125
29. Patel JK, Jaiman RS, Soni NV, Zapadiya DM (2026) Survey on common scab of potato caused by
30. spp. in North Gujarat, India. Indian Phytopathology
31. Qiao G, Xiao SY, Dong J, Yang Q, Che HY, Sun XC (2026) The Multifaceted Functions of Plant Asparagine Synthetase: Regulatory Mechanisms and Functional Diversity in Growth and Defense. Plants-Basel, 15
32. Quast C, Pruesse E, Yilmaz P, Gerken J, Schweer T, Yarza P, Peplies J, Glöckner FO (2013) The SILVA ribosomal RNA gene database project: improved data processing and web-based tools. Nucleic Acids Res 41:D590–D596
33. Rabbee MF, Ali MS, Choi J, Hwang BS, Jeong SC, Baek KH (2019) Bacillus velezensis: A Valuable Member of Bioactive Molecules within Plant Microbiomes. Molecules, 24
34. Rabbee MF, Baek KH (2020) Antimicrobial Activities of Lipopeptides and Polyketides of for Agricultural Applications. Molecules, 25
35. Rabbee MF, Hwang BS, Baek KH (2023) A Beneficial Biocontrol Agent or Facultative Phytopathogen for Sustainable Agriculture, vol 13. Agronomy-Basel
36. Saiyam D, Dubey A, Malla MA, Kumar A (2024) Lipopeptides from Bacillus: unveiling biotechnological prospects-sources, properties, and diverse applications. Brazilian J Microbiol 55:281–295
37. Shafi Z, Shahid M (2025) Root exudates as molecular architects shaping the rhizobacterial community: A review, vol 36. Rhizosphere
38. Shi WC, Li MC, Wei GS, Tian RM, Li CP, Wang B, Lin RS, Shi CY, Chi XL, Zhou B, Gao Z (2019) The occurrence of potato common scab correlates with the community composition and function of the geocaulosphere soil microbiome. Microbiome, 7
39. Tao H, Wang SS, Li XY, Li XB, Cai JY, Zhao LF, Wang J, Zeng J, Qin YZ, Xiong XY, Cai YF (2023) Biological control of potato common scab and growth promotion of potato by
40. Y6 Frontiers in Microbiology, 14
41. Wang H, Liu RJ, You MP, Barbetti MJ, Chen YL (2021) Pathogen Biocontrol Using Plant Growth-Promoting Bacteria (PGPR): Role of Bacterial Diversity, vol 9. Microorganisms

42. Wu X, Wu X, Shen L, Li J, Yu R, Liu Y, Qiu G, Zeng W (2019) Whole Genome Sequencing and Comparative Genomics Analyses of Pandoraea sp. XY-2, a New Species Capable of Biodegrade Tetracycline. Front Microbiol 10:33
43. Zeng J, Liu XJ, Song L, Lin XG, Zhang HY, Shen CC, Chu HY (2016) Nitrogen fertilization directly affects soil bacterial diversity and indirectly affects bacterial community composition. Soil Biol Biochem 92:41–49
44. Zhang J, Liu W, Bu J, Lin Y, Bai Y (2023) Host genetics regulate the plant microbiome. Curr Opin Microbiol 72:102268
45. Zhang Z, Tan W, Liu J, Long J, Zhai Z, Feng Y, Wei L, Du H, Fu Q, Pu Y, Wang P, Zhang C, Zhu G (2026) Metabolomic remodeling and genetic regulation in potato tubers during domestication. Mol Plant 19:328–345
46. Zhao P, Liu L, Cao J, Wang Z, Zhao Y, Zhong N (2022) Transcriptome Analysis of Tryptophan-Induced Resistance against Potato Common Scab. Int J Mol Sci, 23
47. Zhao T, Vink SN, Jia X, Erban A, Schaarschmidt S, Kopka J, Zuther E, Treder K, Michalowska D, Guyoneaud R, Elzenga JTM, Attard E, Salles JF (2025) Unveiling Potato Cultivars With Microbiome Interactive Traits for Sustainable Agricultural Production. Plant Cell Environ
48. Zhong X, Jin Y, Ren H, Hong T, Zheng J, Fan W, Hong J, Chen Z, Wang A, Lu H, Zhong K, Huang G (2024) Research progress of Bacillus velezensis in plant disease resistance and growth promotion. Front Industrial Microbiol, 2
49. Zhou X, Wang J, Liu F, Liang J, Zhao P, Tsui CKM, Cai L (2022) Cross-kingdom synthetic microbiota supports tomato suppression of Fusarium wilt disease. Nat Commun 13:7890
50. Zhou Y, Wang H, Sun J, Wicaksono WA, Liu C, He Y, Qin Y, Berg G, Li L, Lin H, Chai Y, Bai Y, Ma Z, Cernava T, Chen Y (2025) Phenazines contribute to microbiome dynamics by targeting topoisomerase IV. Nat Microbiol 10:2396–2411

Figures

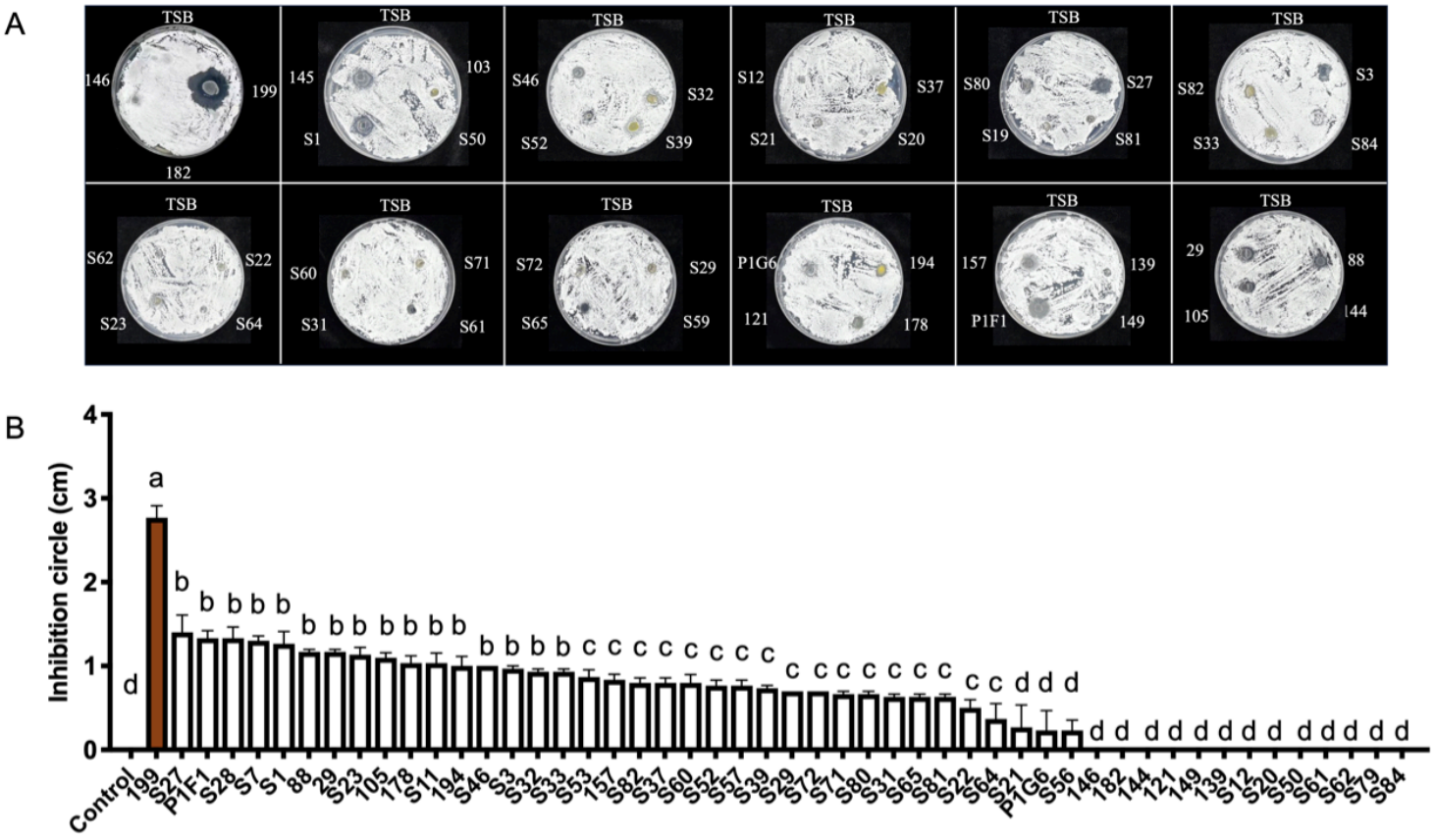

Figure 1

Screening of antagonistic activity among *Bacillus*isolates. **A** Antagonistic phenotypes of 51 *Bacillus* isolates grown on TSB medium, with inhibition zones indicating suppression of the target pathogen. **B** the Quantitative analysis of inhibition zone diameters for all tested isolates. The red bar indicates the isolate with the strongest antagonistic activity. Data are presented as mean ± SE (n = 3). Significant differences among isolates were determined by one-way ANOVA followed by Tukey's HSD multiple comparison test. Different letters indicate significant differences at $P < 0.05$.

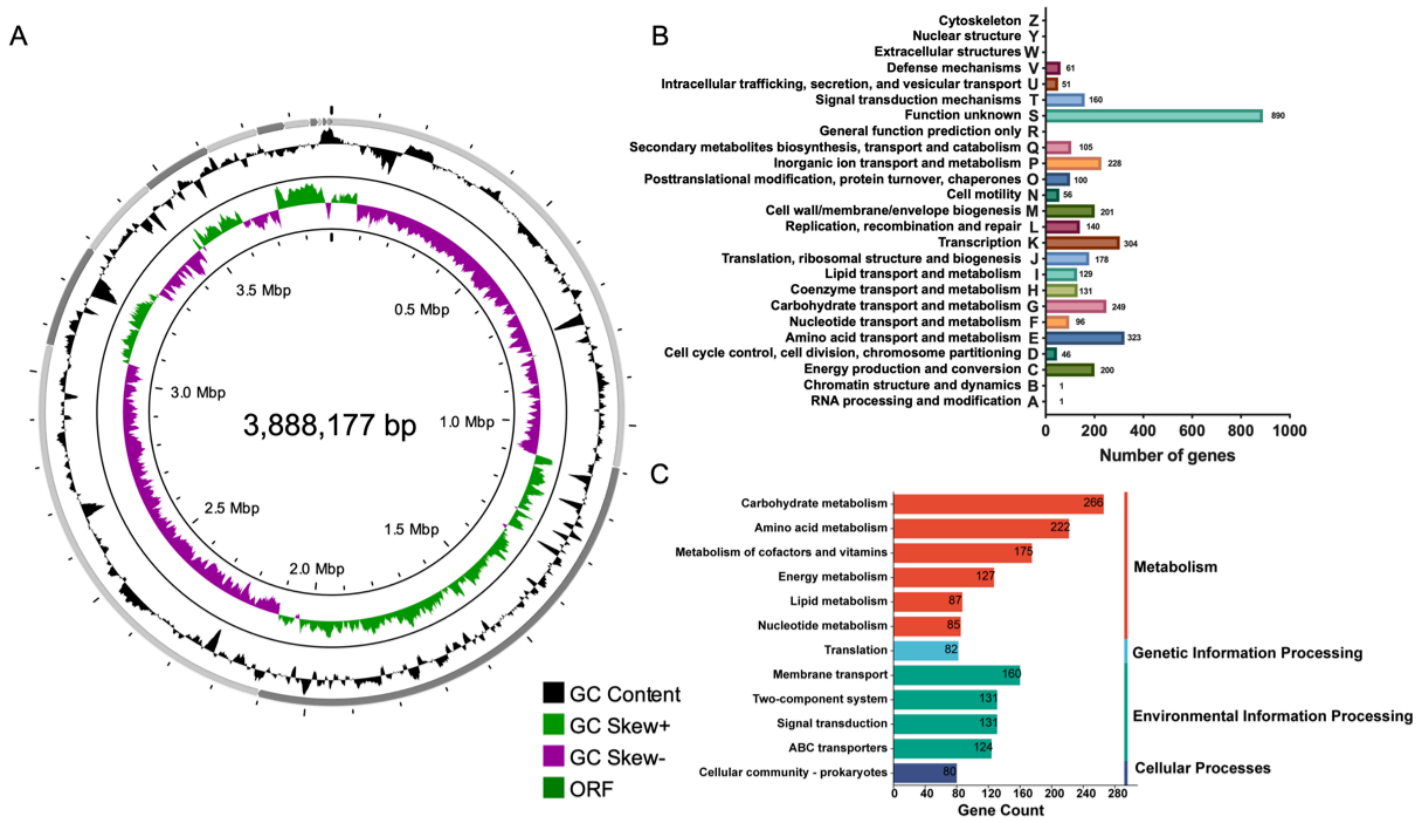

Figure 2

Genomic features and function prediction of *B. velezensis* 199. **A** Circular genome map of strain 199 generated using CG View. **B** COG functional classification of protein-coding genes in the genome of strain 199. **C** KEGG pathway annotation of genes in the genome of strain 199.

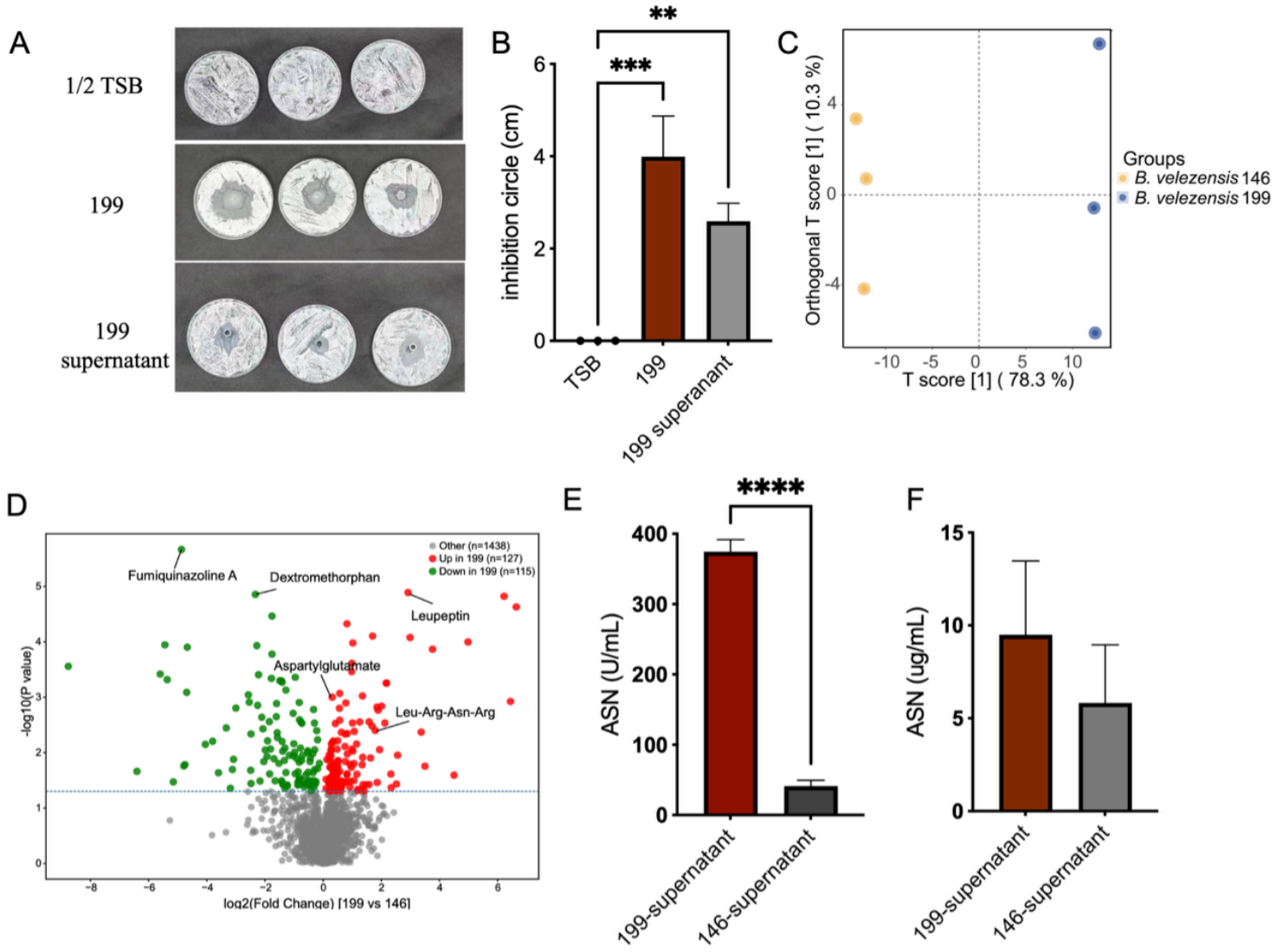

Figure 3

Antagonistic activity and metabolomic profiling of the cell-free supernatant of *B. velezensis* 199. **A** *In vitro* antagonistic activity of strain 199 and its cell-free supernatant against the potato common scab pathogen. 1/2 TSB medium was used as the control. **B** Quantification of inhibition zones produced by half-strength TSB, live strain 199, and the cell-free supernatant of strain 199. Data are shown as means ± SE. Asterisks indicate significant differences according to student *t*-test: ***P* < 0.01, ****P* < 0.001. **C** Orthogonal partial least-squares discriminant analysis (OPLS-DA) score plot showing the metabolic separation between the cell-free supernatants of strain 199 and the non-antagonistic strain strain 146. **D** Volcano plot showing differentially accumulated metabolites in the cell-free supernatant of strain 199 compared with that of strain 146. Red dots indicate metabolites with significant changes based on both *P* value and $\log_2$FC; green dots indicate metabolites meeting the $\log_2$FC threshold only; purple dots indicate metabolites meeting the *P*-value threshold only (*P* < 0.05); gray dots indicate non-significant metabolites. Representative enriched metabolites are labeled. The Asparaginase (**E**) and ASN content (**F**) in supernatant of strain 199 and strain 146. *B. velezensis* 146, a negative control.

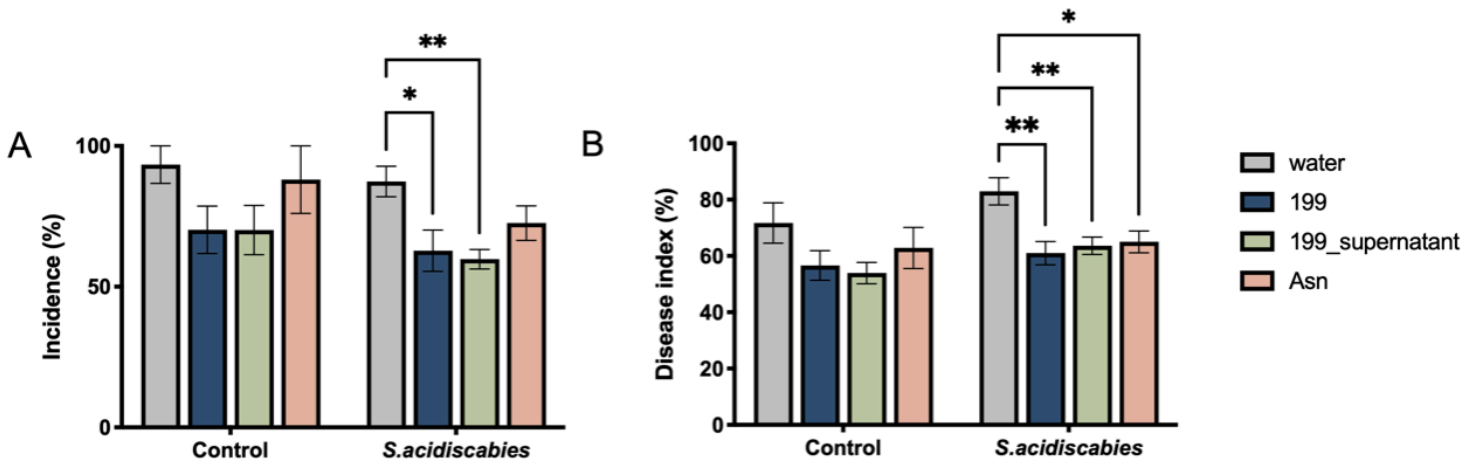

Figure 4

Biocontrol efficacy of *B. velezensis* 199, cell-free supernatant of *B. velezensis*199, and asparagine under greenhouse condition. **A** Disease incidence of potato tubers under different treatments. **B** Disease index of potato tubers under different treatments. Data are shown as means ± SE. Statistical significance was determined by two-way ANOVA followed by Dunnett's multiple comparison test, comparing each treatment with the corresponding water control within the same inoculation condition. Asterisks indicate significant differences from the corresponding water control (*$P < 0.05$, **$P< 0.01$)

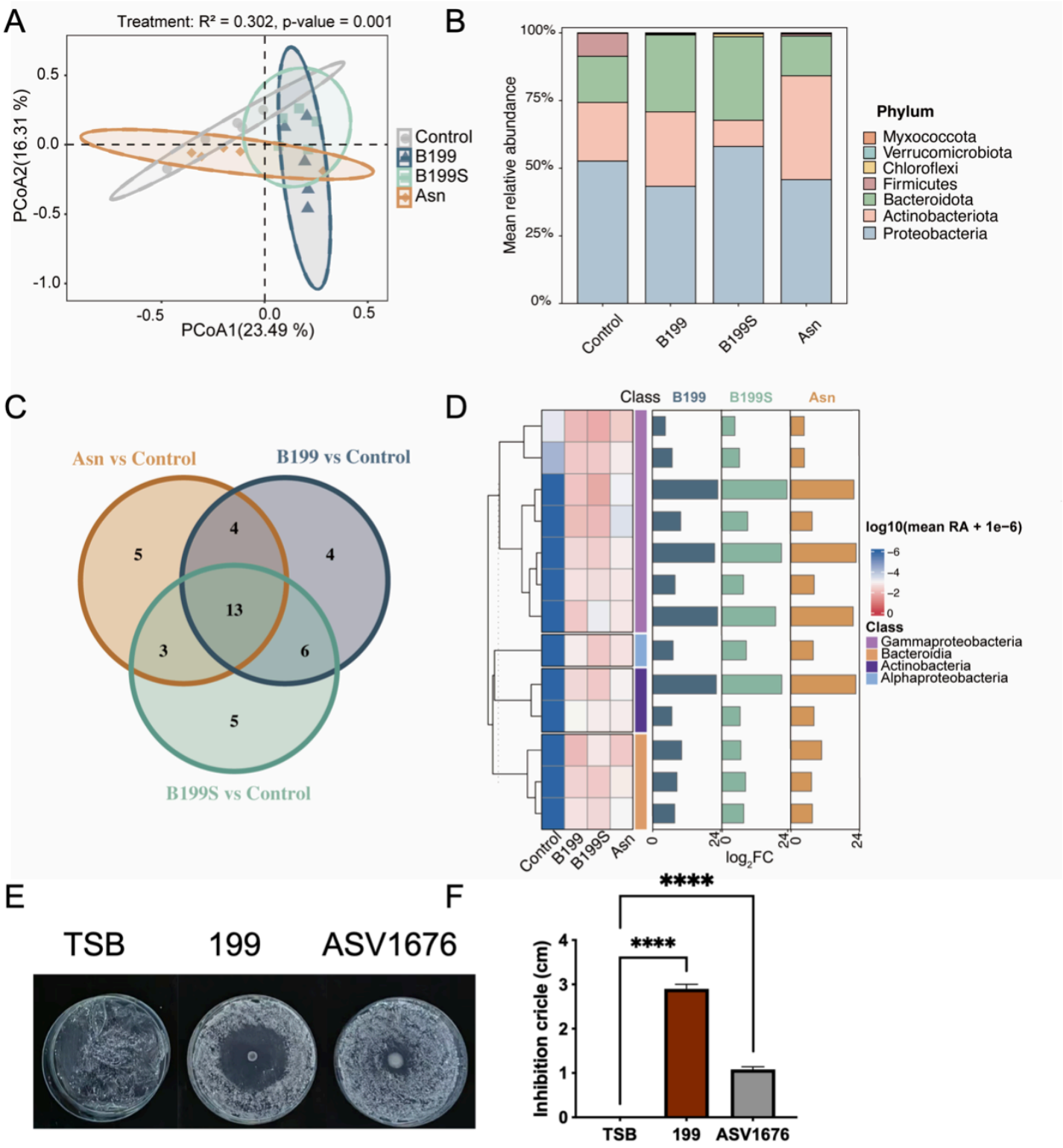

Figure 5

Effects of strain 199, its cell-free supernatant, and asparagine on the potato tuber skin microbiome and enrichment of antagonistic bacteria. **A** Principal coordinate analysis (PCoA) based on Bray–Curtis dissimilarity showing differences in tuber skin bacterial community composition among the control, *B. velezensis* 199 (B199), cell-free supernatant (B199S), and asparagine (Asn) treatments. The overall treatment effect was evaluated using PERMANOVA (R^2 = 0.302, P = 0.001). **B** Mean relative abundance

of dominant bacterial phylum across the four treatments. **C** Venn diagram showing the overlap of significantly enriched amplicon sequence variants (ASVs) identified by DESeq2 in comparisons of B199, B199S, and Asn with the control (adjusted $P < 0.05$ and $\log_2$ fold change > 1). A total of 13 ASVs were commonly enriched across all three treatments. **D** Heatmap showing the mean relative abundance of the 13 shared enriched ASVs across treatments, with corresponding taxonomic classification at the class level and DESeq2-estimated $\log_2$ fold changes for each treatment relative to the control. Relative abundance values were $\log_{10}$-transformed after addition of a pseudocount (10^{-6}). **E** Antagonistic activity of *B. velezensis* 199 and a *Pandoraea* sp. isolate corresponding to ASV1676 against *Streptomyces acidiscabies*. Tryptic soy broth (TSB) served as the negative control. **F** Quantification of inhibition zone diameters produced by *B. velezensis* 199 and the ASV1676-associated *Pandoraea* sp. isolate against *S. acidiscabies*. **** indicates $P < 0.0001$.

Supplementary Files

This is a list of supplementary files associated with this preprint. Click to download.

- Supplementaryfiles.docx